FULL PAPER

ADVANCED FUNCTIONAL MATERIALS

DOI: 10.1002/adfm.200700038

Co_3O_4 Nanostructures with Different Morphologies and their Field-Emission Properties**

By *Binni Varghese*, *Teo Choon Hoong*, *Zhu Yanwu*, *Mogalahalli V. Reddy*, *Bobba V. R. Chowdari*, *Andrew Thye Shen Wee*, *Tan B. C. Vincent*, *Chwee Teck Lim*,* and *Chorng-Haur Sow**

We report an efficient method to synthesize vertically aligned Co_3O_4 nanostructures on the surface of cobalt foils. This synthesis is accomplished by simply heating the cobalt foils in the presence of oxygen gas. The resultant morphologies of the nanostructures can be tailored to be either one-dimensional nanowires or two-dimensional nanowalls by controlling the reactivity and the diffusion rate of the oxygen species during the growth process. A possible growth mechanism governing the formation of such nanostructures is discussed. The field-emission properties of the as-synthesized nanostructures are investigated in detail. The turn-on field was determined to be 6.4 and 7.7 $V\,\mu m^{-1}$ for nanowires and nanowalls, respectively. The nanowire samples show superior field-emission characteristics with a lower turn-on field and higher current density because of their sharp tip geometry and high aspect ratio.

1. Introduction

Nanostructured materials with tunable characteristics, such as chemical composition, relative size, and morphological structure, have great potential from a fundamental as well as a technological viewpoint. Recent demonstrations of the application of nanostructures as electron field emitters,[1] functional nanoelectronic components,[2] and chemical or biological sensor elements[3] have an invigorating influence on nanomaterials research. Among the wide variety of research activities on nanomaterials, nanostructure-based field emitters have attracted much attention because of their great commercial potential. Carbon nanotubes (CNT) have long been recognized as an excellent field emitter with a low turn-on field and high current density.[4] However, some of the challenges involved in the development of CNT emitters include uncertainty in their electronic properties, and difficulties involved in their manipulation and integration into devices. Several researchers have focused their effort on the search for alternate field-emitting materials. Studies on semiconducting oxide nanostructures have shown great promise in this direction.[5]

Cobalt oxides belong to the family of transition-metal oxides and the most stable phase, Co_3O_4, is an intrinsic p-type semiconductor (direct optical bandgaps at 1.48 and 2.19 eV).[6] The chemical stability of Co_3O_4 over a wide temperature range and its high mechanical strength (Young's modulus ≈ 116–160 GPa) render this material a potential candidate for field emitters. The field-emission (FE) properties of Co_3O_4 nanostructures, however, have not been investigated in detail. Cobalt oxide nanoparticles have exhibited outstanding electrochemical,[7] magnetic,[8] catalytic,[9] and gas sensing[10] capabilities. In recent years, the synthesis and structural characterization of cobalt oxide nanostructures have been reported.[11] More recently, Nam et al. demonstrated the feasibility of employing viruses to synthesize and assemble cobalt oxide nanowires as an electrode material (anode) for lithium-ion batteries.[12] In an earlier report, our group demonstrated an approach to synthesize aligned cobalt oxide 2D nanostructures (nanowalls) by direct heating of a cobalt foil using a hotplate under ambient conditions and we investigated their FE properties.[13] However, the hotplate technique is limited to the formation of simple 2D nanostructures. Rational synthetic approaches to form different nanostructures are highly desirable to fully exploit the potential offered by the reduced dimensionality.

In this Full Paper, we report a facile method to synthesize vertically aligned, single-crystalline 1D (nanowires) or 2D

[*] Prof. C. T. Lim, Prof. C.-H. Sow, B. Varghese, T. C. Hoong, Dr. Z. Yanwu, Prof. A. T. S. Wee, Prof. T. B. C. Vincent
National University of Singapore Nanoscience and Nanotechnology Initiative (NUSNNI)
2 Science Drive 3, Singapore 117542 (Singapore)
E-mail: mpelimct@nus.edu.sg
Prof. C.-H. Sow, B. Varghese, T. C. Hoong, Dr. Z. Yanwu, Dr. M. V. Reddy, Prof. B. V. R. Chowdari, Prof. A. T. S. Wee
Department of Physics, Faculty of Science
National University of Singapore
2 Science Drive 3, Singapore 117542 (Singapore)
E-mail: physowch@nus.edu.sg
Prof. C. T. Lim
Division of Bioengineering
National University of Singapore
Blk E3A, 9 Engineering Drive 1, Singapore 117576 (Singapore)
Prof. C. T. Lim, Prof. T. B. C. Vincent
Department of Mechanical Engineering
National University of Singapore
9 Engineering Drive 1, Singapore 117576 (Singapore)

[**] Supporting Information is available online from Wiley InterScience or from the authors.

ADVANCED FUNCTIONAL MATERIALS

(nanowalls) structures of Co_3O_4 on a metal foil. This method involves the reaction of gaseous oxygen with pre-annealed cobalt foils to form Co_3O_4 nanostructures that naturally self-assemble on the cobalt foil. The growth temperature is relatively low and is far below the evaporation temperature of cobalt. The morphology variations of the nanostructures were achieved by varying the reactivity and diffusivity of oxygen via the creation of a plasma environment in the system. The direct growth of quasi-aligned nanostructures on the cobalt foils makes the samples excellent test candidates for field-emission performance. This approach eliminates further post-growth manipulation and assembly of the nanomaterials for FE characterization. The FE properties of the as-synthesized Co_3O_4 nanostructures were studied in detail to explore the morphological effect on the emission characteristics.

2. Results and Discussion

Two different procedures were adopted for the synthesis of cobalt oxide nanostructures. In the first case, cobalt foils were initially heated to 450 °C on a heating coil in a vacuum chamber at a base pressure of $\approx 1 \times 10^{-6}$ Torr (1 Torr = 133.3 Pa). Oxygen gas was introduced into the chamber at a flow rate of 30 sccm. During growth, pressure inside the chamber was maintained at 1 Torr and the growth time was set for 3 h. The growth was terminated by stopping the oxygen leak into the system followed by pumping away the remaining oxygen from the chamber. The samples were then cooled down naturally to room temperature. In the second approach, a 200 W radio frequency (RF) plasma was introduced to create an oxygen plasma in the chamber, while all other conditions were identical to the first experiment. Figure 1a and b shows scanning electron microscopy (SEM) images of the cobalt foil heated in oxygen gas. The foils were observed to be uniformly covered with nanowires, aligned perpendicularly to the substrate surface. The as-grown nanowires have diameters in the range of 10 to 50 nm and are 2–10 μm in length. Figure 1c and d shows SEM images of the nanostructures formed on the cobalt foil heated in the presence of oxygen plasma. These 2D nanowall-type structures are also vertically aligned with a wall thickness typically in the range of 20–40 nm. The vertical height of the nanowalls are in the range of 0.5–1.5 μm and the horizontal length can be up to 3 μm. Recently, we have reported similar morphologies for cobalt oxide formed by direct heating of cobalt foil in ambient conditions using a hotplate.[13] With the new approach adopted in this work, we were able to controllably and exclusively synthesize Co_3O_4 nanowires and nanowalls. Also, the uniformity of the nanowalls has been improved significantly in this new method. In addition, the growth duration is extremely short in comparison to the previous work. The number densities of nanowires and nanowalls were calculated to be 7×10^7 and 4×10^8 per square centimeter, respectively, from the SEM images. It should be noted that we have also carried out a systematic investigation by growing the nanostructures using oxygen plasma generated at different RF power values (Supporting Information, Fig. S1) and at different temperatures (Supporting Information, Fig. S2). With an RF plasma of 50–100 W, foil samples covered with a mixture of Co_3O_4 nanowires and nanowalls were formed (Fig. S1). However, the process using an RF power of 200 W generated cobalt oxide nanowalls exclusively. In the temperature studies (Fig. S2), we found that growth at a lower temperature produced nanostructures with a low number density and poor uniformity.

Here, we have further demonstrated that the cobalt oxide nanostructures can be synthesized directly on a wide variety of substrates. By using substrates with a thin film of cobalt, it is possible to grow cobalt oxide nanostructures on various supporting platforms. To this end, substrates like silicon, stainless steel, and so on, were coated with cobalt (≈ 300 nm thick) using an RF magnetron sputtering system. These substrates were then heated in the respective conditions for the growth of cobalt oxide nanowires or nanowalls, as described earlier. SEM imaging revealed that these substrates were covered with the expected nanostructures.

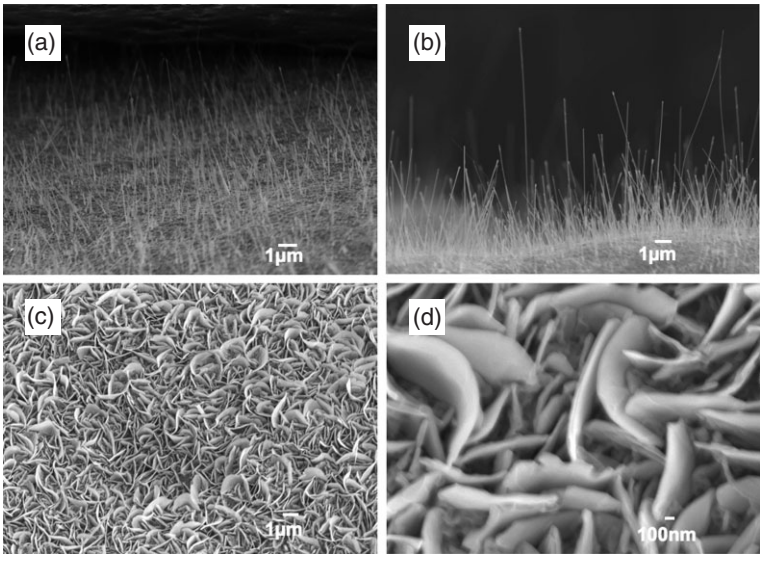

Figure 1. Scanning electron microscopy (SEM) images of vertically aligned cobalt oxide nanowires grown on cobalt foil, viewed at a) 20° and b) 90° from the substrate normal. c, d) SEM images of cobalt oxide nanowalls grown by oxygen plasma treatment on a cobalt foil, viewed at 20° from the substrate normal.

The crystal structures of the as-synthesized cobalt oxide nanostructures were identified by X-ray diffraction (XRD). Figure 2 displays the XRD patterns of cobalt oxide nanostructures on cobalt foil (Fig. 2a and b) and on a Si(100) substrate (Fig. 2c and d). The peaks in the XRD patterns were indexed on the basis of a spinel structure assuming the space group *Fd*3*m* (Co_3O_4: Joint Committee on Powder Diffraction Standards (JCPDS) card no.: 76-1802; CoO: JCPDS card no.: 78-0431; Co metal: JCPDS card no.: 01-1152). The XRD patterns of the nanowires and nanowalls on cobalt foils show a Co_3O_4 phase in addition to CoO and Co phases (peaks due to substrate). For more clarity and also to avoid additional peaks from the cobalt foil, the XRD patterns of the

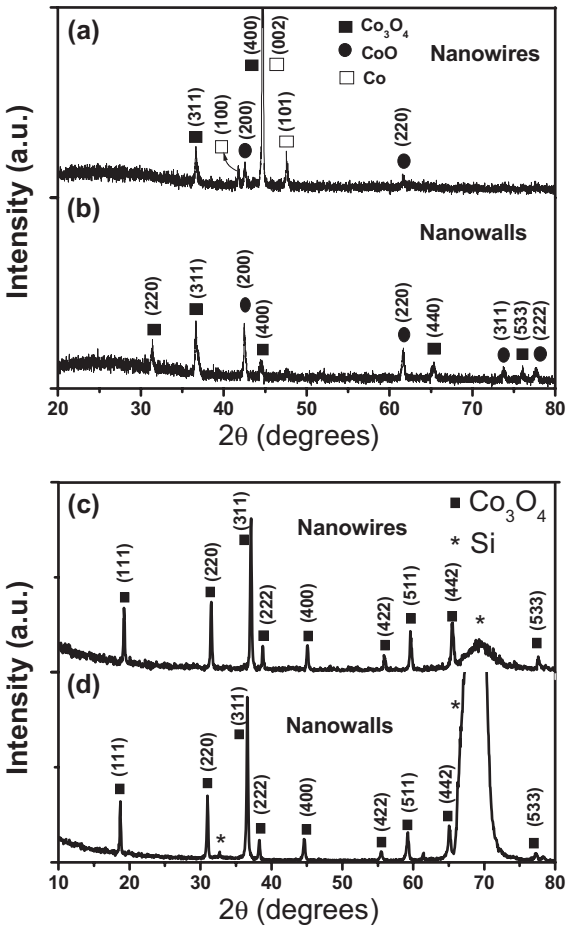

Figure 2. XRD patterns of cobalt oxide nanowires and nanowalls on a, b) cobalt foil and c, d) a Si(100) substrate. Miller indices (*hkl*) are shown.

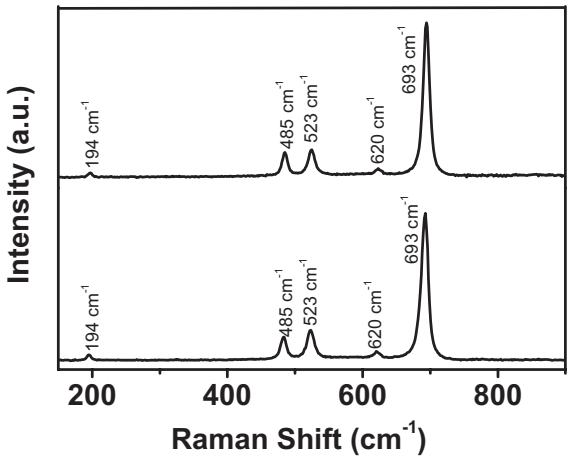

Figure 3. Micro-Raman spectra of cobalt oxide nanowires (upper) and nanowalls (lower).

nanowires and nanowalls on a Si(100) substrate (Fig. 2c and d) were recorded. The XRD patterns show a single phase with lattice parameter $a = 8.071$ and 8.073 Å for nanowires and nanowalls, respectively. The obtained lattice parameters are in good agreement with the reported value of Co_3O_4 powder ($a = 8.072$ Å; JCPDS: 76-1802). In conclusion, the XRD patterns of both nanowires and nanowalls on cobalt foil contain minor peaks indicating the presence of trace amounts of CoO and Co phases, which are probably formed in the early stage of growth or are substrate peaks. Whereas the XRD patterns of the Co_3O_4 nanostructures on the Si(100) substrate are a good indication of a well-ordered spinel structure.

The micro-Raman spectra of the cobalt oxide nanostructures were recorded at room temperature. Cobalt oxide nanowire and nanowall samples show identical Raman lines, as shown in Figure 3. The five prominent Raman peaks observed correspond to the A_{1g} (693 cm^{-1}), F_{2g} (620 cm^{-1}), F_{2g} (523 cm^{-1}), E_g (485 cm^{-1}), F_{2g} (194 cm^{-1}) modes of the crystalline Co_3O_4 phase and are in agreement with a previous report.[14]

To further elucidate the chemical composition of the as-synthesized nanostructures, X-ray photoelectron spectroscopy (XPS) measurements were carried out. The cobalt foils with nanostructures were dried thoroughly at room temperature in a vacuum chamber ($\approx 10^{-6}$ Torr) to remove the adsorbed water molecules prior to the XPS measurement. Samples covered with nanowires as well as nanowalls show identical peaks within the resolution limits of the instrument (Fig. 4). The O 1s XPS spectra peak with a binding energy (BE) of approximately 530 eV corresponds to oxygen species in the spinel cobalt oxide phase (Co_3O_4).[15] The peak observed close to 532 eV in the O 1s spectra indicate the presence of –OH (hydroxyl) species adsorbed on the surface due to our ex situ experimental conditions. The Co 2p XPS spectra show two major peaks with BE values at 795.6 and 780.2 eV, corresponding to the Co $2p_{1/2}$ and Co $2p_{3/2}$ spin-orbit peaks, respectively, of the Co_3O_4 phase.[16] The Co $2p_{1/2}$–Co $2p_{3/2}$ energy separation is approximately 15.4 eV. Lack of prominent shake-up satellite peaks in the Co 2p spectra further suggests the presence of mainly Co_3O_4 phase.[17] Thus, from BE measurements for O 1s and Co 2p core levels and the spectral shape of the XPS spectra, it is clear that the nanostructures formed are composed of Co_3O_4.

Detailed investigations of the microstructures of the as-grown cobalt oxide nanostructures were performed using transmission electron microscopy (TEM). The nanostructure suspension was first prepared by sonicating heated metal foil in ethanol (99.9 %). This suspension was subsequently used for dip-coating to transfer some of these nanostructures onto commercially available carbon-coated copper TEM grids. These grids were dried in air and then used for the TEM studies. Figure 5a shows a typical TEM image of a cobalt oxide nanowire (diameter ≈ 30 nm), which is shown to be essentially straight and possesses a more or less uniform cross section throughout its length. The high-resolution TEM (HRTEM) image (Fig. 5b) reveals fringes perpendicular to the nanowire axis and clearly indicates its single-crystalline nature. The measured lattice spacing is 2.83 Å, corresponding to the interlayer spacing of the (220) planes of Co_3O_4 ($d = 2.86$ Å). Figure 5c shows a TEM image of an isolated nanowall, and Figure 5d shows its typical HRTEM image. The layered structure visible in the

ADVANCED FUNCTIONAL MATERIALS

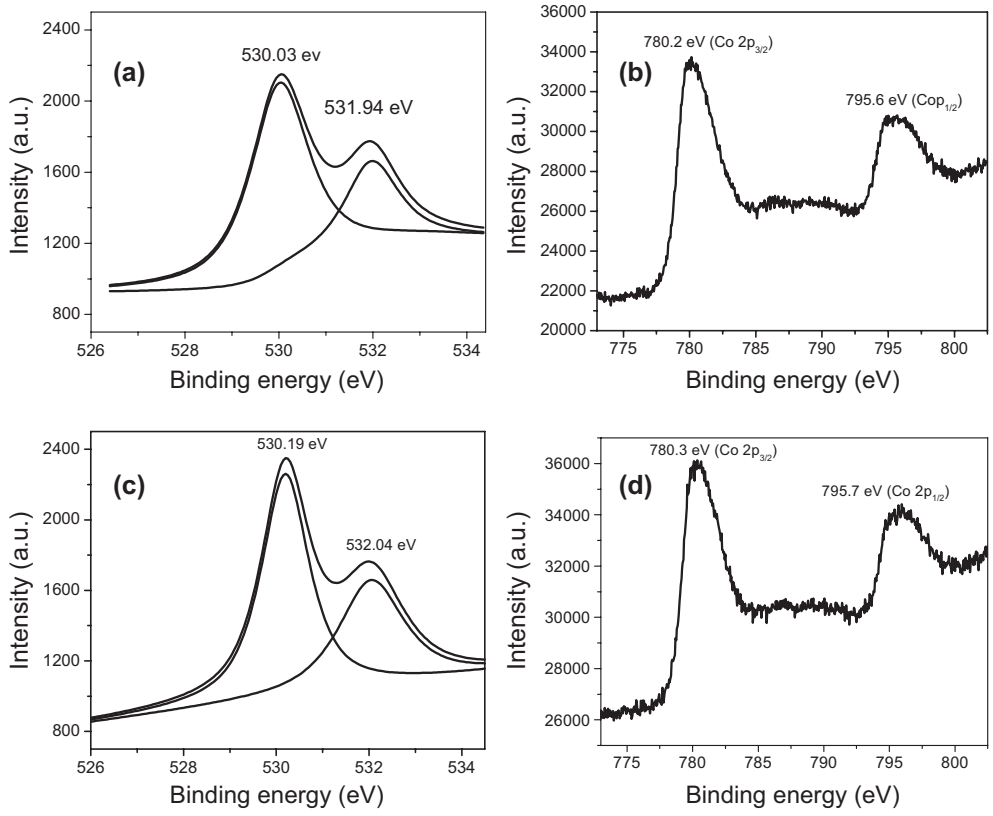

Figure 4. XPS measurements for the a, c) O 1s and b, d) Co 2p core levels for nanowires (upper spectra) and nanowalls (lower spectra).

TEM image of the nanowall is perhaps due to fast growth in different lattice directions. The measured lattice spacings of 2.42 and 2.32 Å are congruent to the lattice spacings of the (311) ($d = 2.43$ Å) and (222) ($d = 2.34$ Å) planes of Co_3O_4, respectively. Figure 5e shows the selected-area electron diffraction (SAED) pattern of the nanowire with zone axis [001]. All the diffraction spots in the SAED pattern can be indexed with the spinel cubic Co_3O_4 phase. The SAED pattern (Fig. 5f) of the nanowalls, however, is more complicated primarily because of its layered structure.

A close-up view of nanowires reveals the presence of a faceted particle at each nanowire tip (Fig. 6a). This suggests that the growth would follow a self-catalytic growth mechanism, which is primarily developed in the context of 1D growth of materials with low-melting-point metal components.[18] The presence of a particle with a high metal content at the tip is often associated with the self-catalyst growth route.[19] However, TEM and energy dispersive X-ray (EDX) spectroscopy inspections of the particle at the tip of the Co_3O_4 nanowires show no significant variations, either in chemical composition or in phase, compared to the main body of the nanowire. Figure 6b shows the HRTEM image of the selected region (as indicated in the inset) at the tip of the nanowire. The measured lattice spacing of 2.46 Å is in good agreement with the (311) interplanar distance of the Co_3O_4 phase ($d = 2.43$ Å). It should be noted that, in HRTEM inspection, we did not observe any twin crystal formation or grain boundary at the neck region connecting the nanowire to its tip particle. EDX examination at different regions along the length of the nanowires (including its tip) confirms that the constituents are only oxygen and cobalt, devoid of other foreign elements (Supporting Information, Fig. S3). Moreover, the atomic weight percentage of oxygen and cobalt remains about the same at the tip as in the main body of the nanowire.

To unravel the growth mechanism of the Co_3O_4 nanostructures a consecutive series of short-term nanowire growth steps was carried out. Following the same growth conditions for the synthesis of nanowires, a cobalt foil was first heated for 5 min and cooled down as described before. The resulting nanostructures were inspected by using SEM. Thereafter, the same sample was heated again for another 5 min for subsequent growth of the nanostructures. Figure 6c shows an SEM image of two short nanowires on the sample after the initial 5 min growth stage, while Figure 6d shows an SEM image of the same area of the sample after an additional 5 min of growth. Evidently, the second growth step resulted in a new segment of nanowires that grew from the tip of the existing nanowires. Noticeably, many of the nanowires on the sample exhibit such double-segment morphology. This suggests two possibilities for the growth of the nanowires. Firstly, the precursors needed for the nanowire growth migrate through the side walls of the nanowires to reach the growth front at the tip. In the second case, cobalt vaporizes and combines with an oxygen species to form cobalt oxide, following a vapor–solid (V–S) route for nanowire forma-

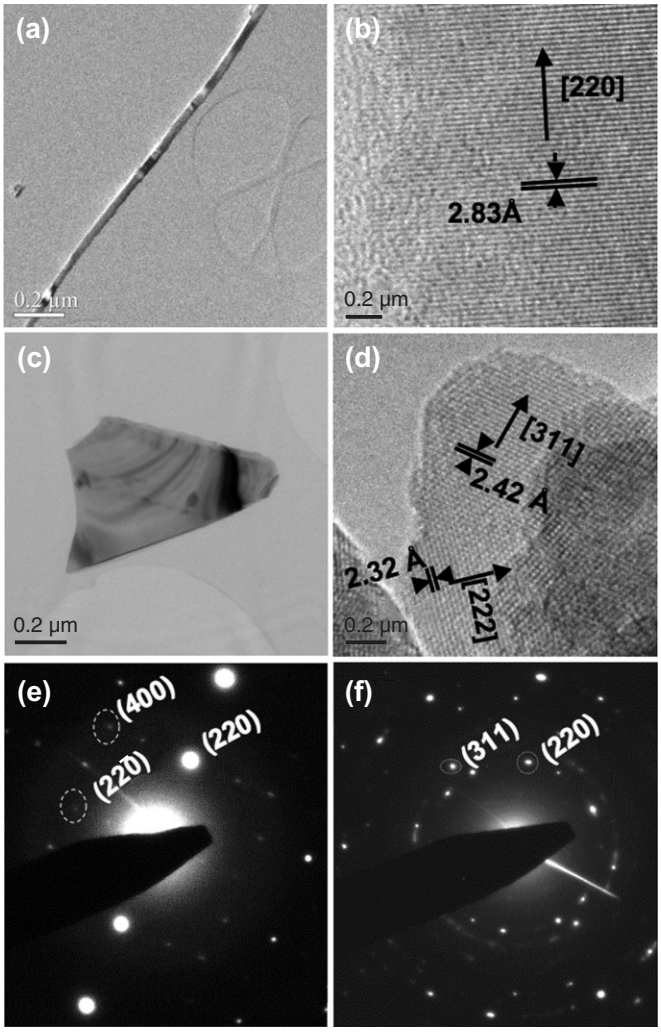

Figure 5. a) Low-resolution TEM image of a cobalt oxide nanowire. b) A typical high-resolution TEM (HRTEM) image of the nanowire near the edge (arrow indicates the growth direction). c) Low-magnification TEM image of the nanowall and d) a typical HRTEM image of the nanowall, showing different growth directions. e, f) Selected-area electron diffraction images of the nanowire and nanowall, respectively.

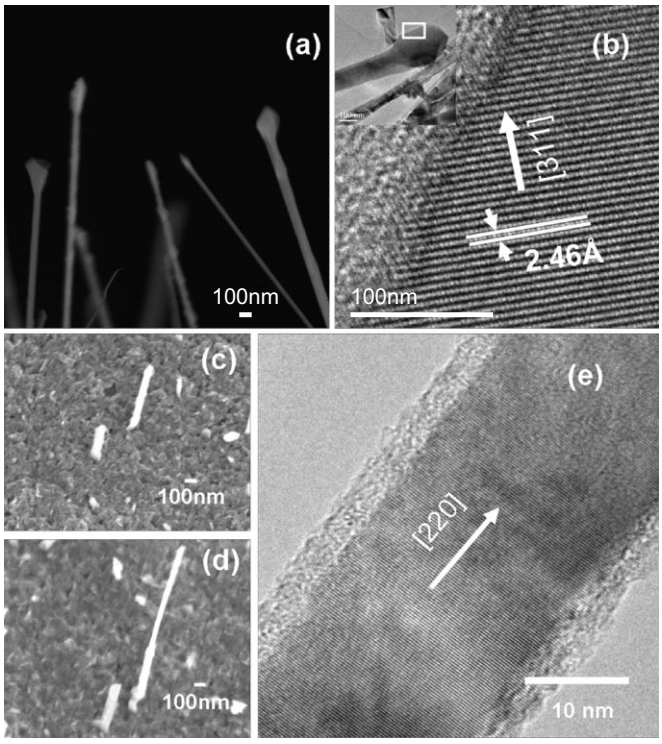

Figure 6. a) Close-up SEM image of Co_3O_4 nanowires, showing the faceted particle at their tips and b) a HRTEM image of such a faceted particle from the highlighted part in the inset. c) SEM image of the cobalt foil with nanowires after 5 min of growth and d) SEM image of the same region of the foil taken after a subsequent 5 min growth. e) A typical TEM image of a Co_3O_4 nanowire, showing the amorphous outer layer.

tion. A very thin (< 3 nm) amorphous layer covering the crystalline core of the nanowire, as revealed by TEM (e.g., Fig. 6e), favors the first possibility. In addition, taking into account the much lower growth temperature compared to the evaporation temperature of cobalt (≈ 1000 °C at 10^{-6} Torr),[20] the V–S route appears to be unlikely.

Based on our experimental results, we propose the following mechanism for the growth of Co_3O_4 nanostructures directly on cobalt foil. Upon heating, a thin layer of Co melt is formed on the surface of the foil due to surface melting. Oxygen from the gaseous phase impinges on this molten surface and undergoes chemical reaction leading to the formation of CoO, Co_3O_4, and so on. Eventually the Co melt becomes saturated with Co_3O_4, leading to the nucleation of cobalt oxide crystallites. Diffusion of oxidizing species and cobalt atoms towards the nucleation sites triggers the kinetically controlled growth along the [220] direction. The advancing front of the nanowire is wrapped with the cobalt melt containing the dissolved oxygen species and various cobalt oxide phases, thus, forming a liquid/solid interface. At this liquid/solid interface the cobalt and oxygen atoms or suboxides of cobalt undergo further chemical reaction to form Co_3O_4. The Co_3O_4 building blocks segregate from the melt and attach to the main body of the nanowire, leading to the rapid growth of nanowire. Thereafter, the growth of the nanowire is predominantly controlled by the migration of oxidizing species and cobalt atoms through the cylindrical body of the nanowire to the tip of the nanowire and the reaction kinetics of formation of Co_3O_4 at the liquid/solid interface of the growing front. It is probable that the formation of the faceted particle at the tip occurs during the gradual cooling after the termination of the growth process. Namely, at a slightly lower temperature, the rapid growth of the nanowires becomes terminated but the molten diffusive materials continue to accumulate at the tip of the nanowires. This accumulated melt becomes crystallites by the epitaxial crystallization of Co_3O_4 from the melt as the temperature of the system further decreases. As a result, the nanowires are found to be capped with a faceted particle.

In a plasma environment, the oxygen species are more reactive. Consequently, the formation events of nucleation sites for cobalt oxide will be higher than in the absence of plasma. In addition, the high diffusion rate of the oxidizing species in the presence of plasma increases the growth rate of nanostructures.

ADVANCED FUNCTIONAL MATERIALS

The high reactivity and diffusivity may cause the rapid growth in different lattice directions leading to the formation of 2D structures. Hence, the morphology switching from 1D (nanowire) to 2D (nanowall) nanostructures is primarily because of the reactivity and diffusivity enhancement of the oxygen species in the plasma.

FE measurements on various Co_3O_4 nanostructures were carried out using a two-parallel-plate configuration in a vacuum chamber at a pressure of 1×10^{-6} Torr. The Co foil with vertically aligned nanostructures was secured to a Cu substrate cathode by copper double-sided tape. Indium tin oxide (ITO) glass coated with a layer of phosphor was employed as the anode. A 100 μm thick polymer film with a small rectangular hole was used as a spacer between the electrodes. The voltage across the electrodes was increased in steps of 5 V up to a maximum of 1100 V and the corresponding emission current was measured using a Keithley 237 high-voltage source measurement unit (SMU). All the FE measurements were performed at room temperature. Figure 7a shows the field-emission current density (J) versus applied field (E) for Co_3O_4 nanowires and nanowalls. When recording data, the applied voltage was repeatedly ramped up and down until there were no significant changes in the J–E plot in between the ramps. The turn-on field, defined as the electric field needed to obtain a field-emission current density of 10 μA cm^{-2}, is 6.4 and 7.75 V μm^{-1} for Co_3O_4 nanowires and nanowalls, respectively. The highest achievable current density is approximately 50 μA cm^{-2} at 7.0 and 8.5 V μm^{-1} for Co_3O_4 nanowires and nanowalls, respectively. The relation between the emission current density with field is given by the Fowler–Nordheim (FN) equation[21]

$$J = \frac{\alpha A}{\phi}(\beta E_{\text{avg}})^2 \exp\left(-\frac{B\phi^{\frac{3}{2}}}{\beta E_{\text{avg}}}\right) \quad (1)$$

where J is the emission current density [A cm^{-2}], E_{avg} is the average electric field [V μm^{-1}], ϕ is the work function of the emitters [eV], α is the area factor, and β is the enhancement factor. A and B are constants, and their values are 1.54×10^{-6} and 6.44×10^3, respectively. The linear variation of $\ln(J/E^2)$ with $1/E$ (FN plot), as shown in Figure 7b, supports the hypothesis that the current is due to field emission, according to FN theory. From the slope of the linear part of the FN plot and using the reported value for the work function (ϕ) of Co_3O_4 (4.5 eV),[22] the enhancement factor β was calculated to be 735 for Co_3O_4 nanowires and 654 for Co_3O_4 nanowalls. Thus, FE measurements show that nanowires with higher aspect ratio can enhance the local field better than nanowalls.[23] However, the β values of nanowires and nanowalls are not significantly different to explain the observed large variation in the current density; this requires a more detailed discussion. In view of the comparatively lower number density of nanowires than nanowalls, the screening effect is likely to be the primary reason for the variation in emission current density. The area factor α is calculated to be 0.665 and 0.227 for Co_3O_4 nanowires and

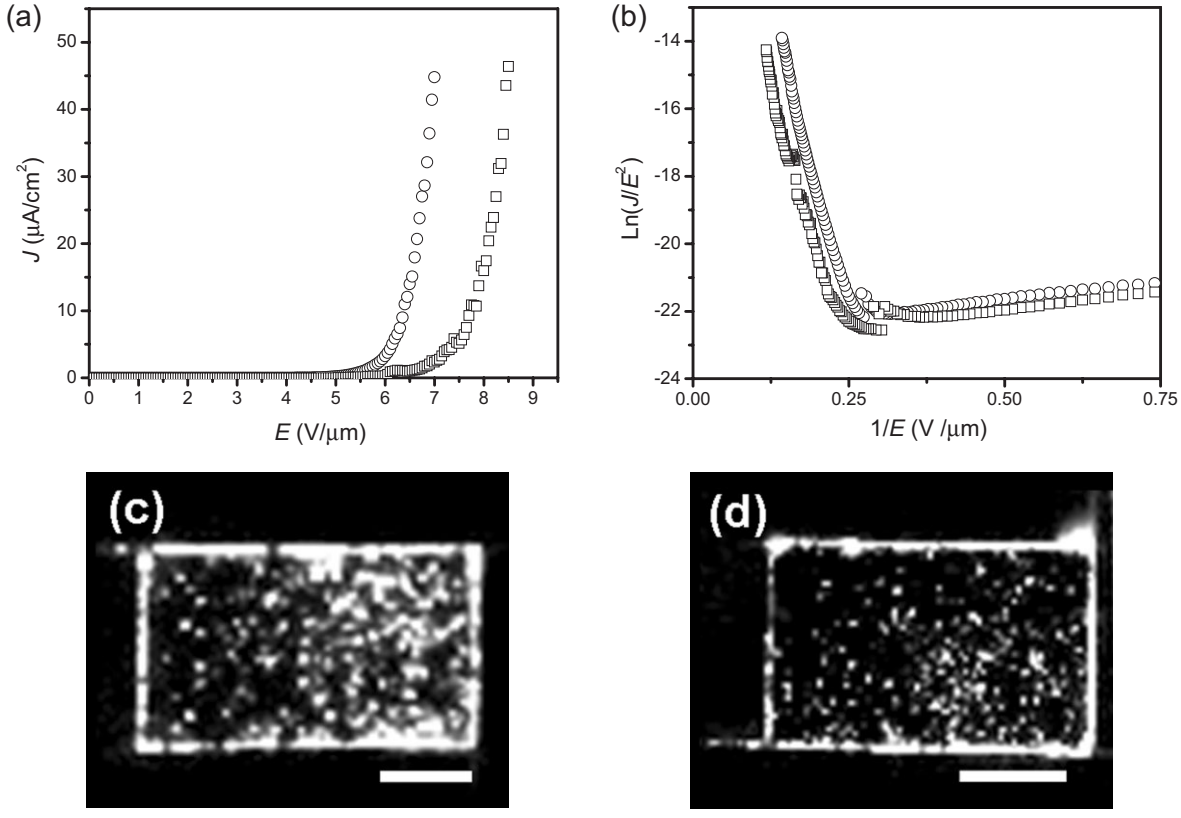

Figure 7. a) FE characteristics of cobalt oxide nanowire (circles) and nanowall (squares) samples. b) FN plots of nanowire and nanowall samples (same symbols). c, d) Fluorescence field-emission images of the nanowires and nanowalls, respectively (scale bars are 2 mm).

nanowalls, respectively. This suggests the higher emission area for Co_3O_4 nanowires could be due to a reduction in the screening effect as the nanowires are spaced further apart than the nanowalls. In addition, the field emission from nanowire and nanowall samples was found to be uniform, justified by the fluorescence images in Figure 7c and d, respectively.

Our FE measurements on the Co_3O_4 nanostructures have shown that nanowires are superior field emitters compared to the nanowalls. The low turn-on field and high current density for the nanowires is attributed to its sharp tip geometry, high aspect ratio, and optimum number density. However, it is worth mentioning that the FE results obtained for nanowall samples in the present study is better than our previous field-emission studies on Co_3O_4 nanowalls grown by direct heating of a cobalt film under ambient conditions.[14] The FE current density of nanowires is adequate for many field-emission device requirements and is comparable with other metal oxide nanostructures.

To illustrate the multifunctionality of the as-synthesized nanostructures, preliminary electrochemical studies on Co_3O_4 nanowalls were carried out by using cyclic voltammetry (CV). CV is a well-adopted electroanalytical technique to study phase transformations, redox couples during the insertion/deinsertion process,[24] and electrode kinetics.[25,26] Cyclic voltammograms were recorded on the cells with Co_3O_4 nanowalls in the potential range of 3.0 to 0.2 V and at a scan rate of 0.1 mV s^{-1}. The CV experiments were carried out at room temperature with Li metal as both the counter and reference electrodes. The cyclic voltammograms of Co_3O_4 nanowalls are shown in Figure 8. During the cathodic scan (Li intercalation into Co_3O_4 nanowalls), a reduction peak occurs at 1.0 V (vs. Li), while during the anodic scan (Li deintercalation from the host), an oxidation peak is shown at 2.1 V (vs. Li). The observed cathodic and anodic peak potentials (redox potentials) are in good agreement with reported CV results on Co_3O_4 thin films.[25] The preliminary CV results demonstrate that Co_3O_4 nanowalls could be used as an anode material for lithium-ion batteries. More detailed electrochemical studies on various morphologies of Co_3O_4 nanostructures, by using galvanostatic discharge–charge cycling, are currently in progress.

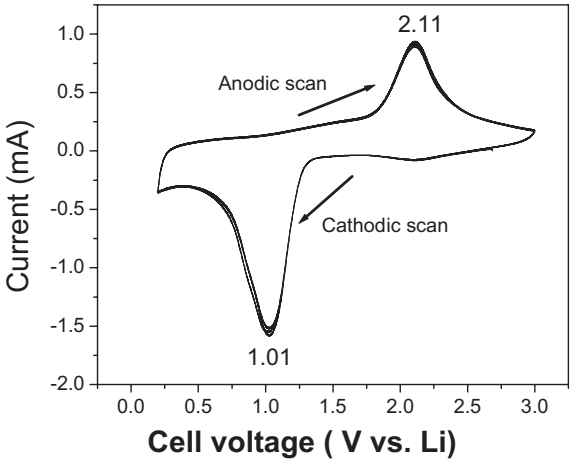

Figure 8. The cyclic voltammograms of Co_3O_4 nanowalls. The cell is represented as Li/1 M $LiPF_6$ (EC:DEC)/Co_3O_4 nanowalls (EC: ethylene carbonate and DEC: diethyl carbonate). Potential scan between 3.0 and 0.2 V; Scan rate: 0.1 mV s^{-1}. Cycles 4–6 are shown.

3. Conclusions

In summary, Co_3O_4 nanostructures with 1D and 2D morphologies were synthesized using a simple method at relatively low temperature. Morphology alteration of the nanostructures was achieved by modifying the reactivity and diffusivity of oxygen via the introduction of a plasma atmosphere. The as-synthesized nanostructures were characterized using XRD, micro-Raman spectroscopy, XPS, and HRTEM analysis. Our synthesis method to create vertically aligned nanostructures has three major advantages; i) the processing temperature is considerably lower, ii) this is a catalyst-free method and hence avoids the sometimes undesirable outcome of incorporation of catalyst particles into the nanostructures; and iii) morphological variations can be readily achieved. In particular, this method was found useful in the synthesis of other metal oxide nanostructures with morphological variations, which will be published elsewhere. Both 1D and 2D Co_3O_4 samples showed promising FE properties and are comparable with other known oxide nanostructures. The nanowires exhibited a lower turn-on field and higher current density compared to the nanowalls. These nanostructures could find application in the future in cold-cathode-based electronics and as an anode material for lithium-ion batteries.

4. Experimental

Cobalt foils (99.95 %) with 0.1 mm thickness were purchased from Alfa Aesar. Pieces of cobalt foil of size 5 mm × 5 mm were used for growing oxide nanostructures. The native oxide layer on the surface of the foil was removed by polishing with sand paper followed by cleaning in ethanol. These samples were dried in air and placed on a metallic base inside a vacuum chamber. The sample temperature could be increased up to a maximum of 600 °C and was measured with a thermocouple, which was kept in contact with the metallic base. A radio frequency (RF) plasma generator (13.6 MHz) with maximum power of 550 W was coupled by way of a parallel-plate electrode to the chamber to create a plasma environment. The vacuum system comprised a rotary and turbo pump and was used to evacuate the chamber to a base pressure of $\approx 1 \times 10^{-6}$ Torr. Co_3O_4 nanowires were synthesized by heating cobalt foils at 450 °C followed by leaking oxygen into the chamber at a flow rate of 30 sccm. During growth, the pressure inside the chamber was maintained at 1 Torr and the growth time was set for 3 h. For synthesizing Co_3O_4 nanowalls, the oxygen plasma was created in the chamber with an RF power of 200 W, all the other conditions being identical to the procedure employed for the nanowire growth. For the growth of Co_3O_4 nanostructures on foreign substrates, a thin film (≈ 300 nm thickness) of cobalt was first deposited on the substrates using an RF magnetron sputtering unit (Denton vacuum Discovery18 system, 150 W). These substrates were heated in the respective conditions for nanowire and nanowall growth.

The morphology and structure of the as-synthesized nanostructures were characterized using field-emission scanning electron microscopy (JEOL, JSM-6700F), high-resolution transmission electron microscopy (JEOL, JEM-2010F, 200 kV), X-ray diffraction (Philips X-ray diffrac-

ADVANCED FUNCTIONAL MATERIALS

tometer, X'PERT MPD; Cu Kα (1.542 Å) radiation; unit cell parameters were determined by using TOPAS-R Software), Raman spectroscopy (Renishaw system2000, 532 nm excitation wavelength), and X-ray photoelectron spectroscopy (ESCA MK II; Mg Kα source). The field-emission measurements were carried out in another vacuum chamber with a base pressure of $\approx 1 \times 10^{-6}$ Torr. A detailed description of the set-up employed for the field-emission measurements have been reported elsewhere [5d,14].

For cyclic voltammetry measurements, the working electrode consisted of Co_3O_4 nanowalls on a stainless steel substrate, used as current collector, and the geometrical area of the electrode was 2.0 cm^2. Note that no conducting carbon or binders were used for the fabrication of the above electrodes. Coin-type test cells (size 2016) were assembled using Co_3O_4 nanowalls as the electrode, Li-metal foil (Kyokuto metal Co. Ltd., Japan) as the counter and reference electrodes, polypropylene (celgard) as the separator, and a 1 M solution of $LiPF_6$ in ethylene carbonate (EC) and diethyl carbonate (DEC) (1:1 by volume; Merck). The cells were fabricated in an argon-filled glove box (MBraun, Germany). More details of cell fabrication have been described elsewhere [27]. The cyclic voltammetry was carried out by using the computer-controlled Macpile II system (Biologic, France).

Received: January 9, 2007
Revised: February 28, 2007
Published online: July 10, 2007

[1] N. S. Xu, S. E. Huq, *Mater. Sci. Eng., R* **2005**, *48*, 47.
[2] Y. Huang, X. Duan, Y. Cui, L. J. Lauhon, K. H. Kim, C. M. Lieber, *Science* **2001**, *294*, 1313.
[3] A. Kolmakov, M. Moskovits, *Annu. Rev. Mater. Res.* **2004**, *34*, 151.
[4] a) S. S. Fan, M. G. Chapline, N. R. Franklin, T. W. Tombler, A. M. Cassell, H. Dai, *Science* **1999**, *283*, 512. b) Y. Saito, S. Uemura, *Carbon* **2000**, *38*, 169. c) N. D. Jonge, J. M. Bonard, *Philos. Trans. R. Soc. London, A* **2004**, *362*, 2239.
[5] a) C. J. Lee, T. J. Lee, S. C. Lyu, Y. Zhang, H. Ruh, H. J. Lee, *Appl. Phys. Lett.* **2002**, *81*, 3648. b) D. Banerjee, S. H. Jo, Z. F. Ren, *Adv. Mater.* **2004**, *16*, 2028. c) S. Q. Li, Y. X. Liang, T. H. Wang, *Appl. Phys. Lett.* **2005**, *87*, 143 104-3. d) Y. W. Zhu, T. Yu, F. C. Cheong, X. J. Xu, C. T. Lim, V. B. C. Tan, J. T. L. Thong, C. H. Sow, *Nanotechnology* **2005**, *16*, 88.
[6] A. Gulino, G. Fiorito, I. Fragalá, *J. Mater. Chem.* **2003**, *13*, 861.
[7] a) P. Poizot, S. Laruelle, S. Grugeon, L. Dupont, J. M. Tarascon, *Nature* **2000**, *407*, 496. b) C. N. P. da Fonseca, M. A. De Paoli, A. Gorenstein, *Adv. Mater.* **1991**, *3*, 553.
[8] a) K. Takada, H. Sakurai, E. T. Muromachi, F. Izumi, R. A. Dilanian, T. Sasaki, *Nature* **2003**, *422*, 53. b) S. Takada, M. Fujii, S. Kohiki, *Nano Lett.* **2001**, *1*, 379.
[9] T. E. Davies, T. García, B. Solsona, S. H. Taylor, *Chem. Commun.* **2006**, 3417.
[10] a) C. Cantalini, M. Post, D. Buso, M. Guglielmi, A. Martucci, *Sens. Actuators B* **2005**, *108*, 184. b) J. Wöllenstein, M. Burgmair, G. Plescher, T. Sulima, J. Hildenbrand, H. Böttner, I. Eisele, *Sens. Actuators B* **2003**, *93*, 442. c) M. Ando, T. Kobayashi, S. Iijima, M. Haruta, *J. Mater. Chem.* **1997**, *7*, 1779.
[11] a) Y. Li, B. Tan, Y. Wu, *J. Am. Chem. Soc.* **2006**, *128*, 14 258. b) T. Li, S. Yang, L. Huang, B. Gu, Y. Du, *Nanotechnology* **2004**, *15*, 1479. c) X. Liu, G. Qiu, X. Li, *Nanotechnology* **2005**, *16*, 3035. d) H. Guan, C. Shao, S. Wen, B. Chen, J. Gong, X. Yang, *Mater. Chem. Phys.* **2003**, *82*, 1002. e) X. Shi, S. Han, R. J. Sanedrin, C. Galvez, D. G. Ho, B. Hernandez, F. Zhou, M. Selke, *Nano Lett.* **2002**, *2*, 289. f) X. Shi, S. Han, R. J. Sanedrin, F. Zhou, M. Selke, *Chem. Mater.* **2002**, *14*, 1897. g) X. Wang, X. Chen, L. Gao, H. Zheng, Z. Zhang, Y. Qian, *J. Phys. Chem. B* **2004**, *108*, 16 401.
[12] K. T. Nam, D. W. Kim, P. J. Yoo, C. Y. Chiang, N. Meethong, P. T. Hammond, Y. M. Chiang, A. M. Belcher, *Science* **2006**, *312*, 885.
[13] T. Yu, Y. Zhu, X. Xu, Z. Shen, P. Chen, C. T. Lim, J. T. L. Thong, C. H. Sow, *Adv. Mater.* **2005**, *17*, 1595.
[14] V. G. Hadjiev, M. N. Iliev, I. V. Vergilov, *J. Phys. C: Solid State Phys.* **1988**, *21*, L199.
[15] L. Armelao, D. Barreca, S. Gross, E. Tondello, *Surf. Sci. Spectra* **2001**, *8*, 14.
[16] a) C. V. Chenck, J. G. Dillard, J. W. Murrray, *J. Colloid Interface Sci.* **1983**, *95*, 398. b) M. Oku, Y. Sato, *Appl. Surf. Sci.* **1992**, *55*, 37.
[17] a) T. J. Chuang, C. R. Brundle, D. W. Rice, *Surf. Sci.* **1976**, *59*, 413. b) M. A. Langell, M. D. Anderson, G. A. Carson, L. Peng, S. Smith, *Phys. Rev. B* **1999**, *59*, 4791.
[18] a) S. N. Mohammad, *J. Chem. Phys.* **2006**, *125*, 094 705. b) E. A. Stach, P. J. Pauzauskie, T. Kuykendall, J. Goldberger, R. He, P. Yang, *Nano Lett.* **2003**, *3*, 867.
[19] Y. X. Chen, L. J. Campbell, W. L. Zhou, *J. Cryst. Growth* **2004**, *270*, 505.
[20] Thin Film Evaporation Materials Reference and Guide, http://www.ee.byu.edu/cleanroom/TFE_materials.phtml?flag=topic_index (accessed February 2007).
[21] R. H. Fowler, L. W. Nordheim, *Proc. R. Soc. London A* **1928**, *119*, 173.
[22] a) B. Klingenberg, F. Grellner, D. Borgmann, G. Wedler, *Surf. Sci.* **1993**, *296*, 374. b) M. R. Castell, S. L. Dudarev, G. A. D. Briggs, A. P. Sutton, *Phys. Rev. B* **1999**, *59*, 7342.
[23] R. C. Smith, J. D. Carey, R. D. Forrest, S. R. P. Silva, *J. Vac. Sci. Technol. B* **2005**, *23*, 632.
[24] K. S. Tan, M. V. Reddy, G. V. Subba Rao, B. V. R. Chowdari, *J. Power Sources* **2005**, *147*, 241.
[25] C. L. Liao, Y. H. Lee, S. T. Chang, K. Z. Fung, *J. Power Sources* **2006**, *158*, 1379.
[26] M. V. Reddy, B. Pecquenard, P. Vinatier, A. Levasseur, *Electrochem. Commun.* **2007**, *9*, 409.
[27] M. V. Reddy, S. Madhavi, G. V. Subba Rao, B. V. R. Chowdari, *J. Power Sources* **2006**, *162*, 1312.